RSC Advances

PAPER

View Article Online
View Journal | View Issue

Cite this: *RSC Adv.*, 2015, **5**, 17076

Osteoblastic cell responses and antibacterial efficacy of Cu/Zn co-substituted hydroxyapatite coatings on pure titanium using electrodeposition method

Yong Huang,*[ab] Xuejiao Zhang,[a] Huanhuan Mao,[b] Tingting Li,[b] Ranlin Zhao,[b] Yajing Yan[b] and Xiaofeng Pang[bc]

Received 10th October 2014
Accepted 3rd February 2015

DOI: 10.1039/c4ra12118j

www.rsc.org/advances

Effective physiological bone integration and absence of bacterial infection are essential for a successful orthopaedic or dental implant. This work elucidated the antibacterial efficacy and cytocompatibility of an electroplated Cu(II) and Zn(II) co-substituted hydroxyapatite (HAP) (*i.e.*, ZnCuHAP) coating on commercially pure titanium (Ti-cp). To improve the antibacterial property of pure HAP, Cu^{2+} was substituted into its structure. Simultaneously, Zn^{2+} is co-substituted as a secondary material into CuHAP to offset the potential cytotoxicity of Cu, because an elevated Cu concentration is toxic. The as-deposited coatings were characterized by Fourier transform infrared spectroscopy, X-ray diffraction, scanning electron microscopy and energy-dispersive X-ray spectroscopy. Co-doping of Zn^{2+} and Cu^{2+} into HAP reduced the porosity, resulting in a denser coating. The Zn^{2+} and Cu^{2+} ions were homogenously co-deposited into HAP films. Potentiodynamic polarisation test revealed that the ZnCuHAP covered coating provided good barrier characteristics and achieved superior corrosion protection for Ti substrates. The as-prepared ZnCuHAP coating was found to be highly effective against *Escherichia coli in vitro*. *In vitro* biocompatibility tests and MTT were employed to assess the cytotoxicity of ZnCuHAP coating with osteoblast-like MC3T3-E1 cells. No adverse effect or cytotoxicity on osteoblasts by Zn/Cu addition was observed, revealing that the co-substitution of Zn in CuHAP efficiently offsets the adverse effects of Cu and improves the performance compared with that of pure HAP.

1. Introduction

Bacterial colony and biofilm formation on the surface of a medical implant is one of the worst possible outcomes of orthopaedic intervention with respect to both patient prognosis and healthcare costs.[1–3] Commercially pure titanium (Ti-cp) and its alloys are used extensively for oral and orthopaedic medical implants because of their low density, high strength, non-toxicity and superior corrosion resistance.[4–6] To enhance bone-bonding ability, metallic implants are generally coated with osteoconductive biomaterials, such as hydroxyapatite (HAP, $Ca_{10}(PO_4)_6(OH)_2$) bioceramics.[7–9] Synthetic HAP is extremely similar to the inorganic component of hard tissues, such as bone and teeth; HAP is also non-toxic at any quantity and osteoconductive.[10–12]

However, the application of pure HAP presents several disadvantages, including a lack of antibacterial activity that affects its long term stability and engenders implant failures.[1,13] This disadvantage induces an increased risk of bacterial adherence and colonization of metallic implants coated with HAP.[13,14] To solve these problems, multiple strategies have been developed to obtain surfaces that are able to reduce the risk of bacterial contamination and promote cell proliferation.[2,13] Introduction of inorganic antibacterial agents into HAP coating has achieved growing attention.[2,14,15] In recent years, incorporation of metallic antibacterial agents (such as Cu^{2+}, Ag^{+}, Ce^{4+} and Zn^{2+}) in bioceramics is mainly implemented because of their antibacterial property, which aids in inhibiting microbial growth at the implant site, and their lack of cytotoxicity at low concentrations.[15–18] Among these ions, Cu(II) is an essential trace element for mammals[2,18] because it stimulates the activity of several enzymes and performs a function in cross-linking of collagen and elastin of bones.[18,19] Cu demonstrates high antibacterial ability by maintaining a low cytotoxicity.[15,18] However, higher content of Cu in the biomaterials has been shown to provide better antibacterial effect, but with increased cytotoxicity.[20] Therefore, incorporating a secondary agent is essential to lessen the adverse effects while maintaining the antimicrobial properties of Cu.[17] Certain minerals such as Zn, Si and Sr, as

[a]*College of Lab Medicine, Hebei North University, Zhangjiakou 075000, China. E-mail: xfpang@aliyun.com; Fax: +86 313 4029150; Tel: +86 18981736790*

[b]*Institute of Life Science and Technology, University of Electronic Science and Technology of China, Chengdu 610054, China*

[c]*International Centre for Materials Physics, Chinese Academy of Science, Shenyang 110015, China*

well as trace amounts of metallic elements, promote bone formation.[6,7,16,21] Among these elements, Zn(II) is one of the most essential trace elements in the mammalian body.[7,21] Zn performs a stimulatory function on osteoblastic proliferation and promotes cell differentiation through the Zn-dependent syntheses in various cell division- and promotion-associated hormones and enzymes.[6,21] Thus, the substitution of Cu in HAP coating could be used to prevent bacterial adherence. In addition, Zn is co-substituted into CuHAP to offset the cytotoxicity of Cu, as well as to provide superior bone bonding capacity.[17,18] However, to the best of our knowledge, reports concerning the deposition of Cu^{2+} and Zn^{2+} (Cu/Zn) co-substituted HAP coating on metallic substrate are scarce.

Numerous papers have reported different HAP coating approaches on metal substrates,[6,9,22] including electrochemical deposition, biomimetic coating, hot isostatic pressing, pulsed laser ablation, sputter coating, dynamic mixing, ion-beam-assisted deposition, sol–gel, thermal spraying, dip coating and plasma spraying process. Amongst these methods, plasma spraying is the only technique that is approved by the Food and Drug Administration.[21,22] However, this approach poses several defects:[9,22] (1) it requires excessively high temperature and costly equipment; (2) it fails to elicit carefully organized growth, so the mineral initiates in non-specific sites; (3) it cannot coat porous surfaces or include bioactive agents; and (4) it has poor substrate-coating bond, which constantly results in many clinical problems. In this sense, electrolytic deposition (ED) has proven to be among the most versatile methods for the synthesis of ion-substituted HAP composite coatings,[6,7] with characteristics that are superior to conventional deposition techniques (*e.g.*, low process temperature, low-cost equipment, probability of fabricating onto porous substrates of complicated shapes and simple control of coating properties). Several studies have reported on the individual substitution of several ions such as Cu, Na, Sr, Mg, Mn, Ag, Zn and F into HAP coating;[6,7,23–30] meanwhile, simultaneous incorporation of Zn and Cu into HAP coating by ED has not been reported. Hence, the present work is designed to fabricate Ti-cp coated with ZnCuHAP to improve antibacterial efficacy, corrosion resistance and cell–biomaterial interactions.

In this study, synthesis of HAP coating substituted with Cu is reported along with the co-substitution of Zn to enhance the antibacterial and biocompatible properties of HAP. An electrolytic deposition technique was adapted to develop Cu/Zn co-substituted HAP coating on Ti-cp.[25–30] The crystallinity, phase purity, level of ionic substitution, and coating morphology of the ZnCuHAP coating was studied. The *in vitro* antibacterial effect of the ZnCuHAP coating was evaluated using *Escherichia coli*. Furthermore, MTT assay was employed to assess the viability of cultured MC3T3-E1 osteoblast precursor cells seeded on pure HAP and ZnCuHAP coatings.

2. Materials and methods

2.1. Preparation of Cu(II)/Zn(II) co-substituted HAP coating

Ti-cp plates (99.9% purity, Non-Ferrous Metals, Ltd., Baoji, China) with dimensions of 10 mm × 10 mm × 0.9 mm were prepared as substrates. The edges of the Ti-cp substrates were rounded to prevent edge effect during ED. Firstly, Ti-cp substrates (100 mm^2 surface) were subjected to fine polishing using SiC paper of different grit sizes (280, 400, 600, 800, 1000 and 2000). Secondly, the samples were etched in a mixed acid ($HNO_3/HCl/H_2O = 1:1:10$, volume ratio) at 25 °C for 15 s to eliminate inherent oxide layers and increase surface roughness. Thirdly, the samples were treated with alkali to enhance hydrophilicity by soaking in 50 mL of 5 M NaOH aqueous solution at 65 °C for 6 h.

In the ED apparatus, saturated calomel electrode, Ti-cp plate, and platinum sheets were designated as the reference, working and auxiliary electrodes, respectively. Analytical-grade calcium nitrate tetrahydrate ($Ca(NO_3)_2 \cdot 4H_2O$), cupric nitrate ($Cu(NO_3)_2 \cdot 3H_2O$), zinc nitrate ($Zn(NO_3)_2 \cdot 6H_2O$), and ammonium dihydrogen phosphate ($NH_4H_2PO_4$) were adopted as the sources for Ca, Cu, Zn and P, respectively. The electrolyte was prepared with a theoretical Ca/P ratio of 1.67 for apatite. The electrolyte solution for deposition, which was composed of analytical-grade 5×10^{-2} M of $Ca(NO_3)_2 \cdot 4H_2O$, 3×10^{-2} M of $NH_4H_2PO_4$, 2×10^{-3} M of $Zn(NO_3)_2 \cdot 6H_2O$, and 2×10^{-3} M of $Cu(NO_3)_2 \cdot 3H_2O$, was maintained at (65 ± 1) °C, and the pH was maintained at 4.3. The coating process was conducted galvanostatically using an electrochemistry workstation (LK2005A, China) at a constant current density of 2 mA cm^{-2} for 25 min.[25,26] After deposition, the ZnCuHAP-coated specimens were carefully rinsed with deionised water. The samples were then immersed in 0.1 M NaOH solution at 65 °C for approximately 4 h, gently rinsed with distilled water, and dried in 65 °C oven for 2 h. The dried films were sintered at 200 °C for 2 h in air. The specimens were cooled down gradually in the oven to decrease stress. For comparison, pure HAP coating was designated as a control.

2.2. Sample characterisation

Topographical features and elemental analysis of the as deposited coatings (HAP and ZnCuHAP) were identified by means of Field Emission Scanning Electron Microscopy (FESEM, JEOL JSM-7500F, Japan) equipped with Energy Dispersive Spectroscopy (EDS). The crystalline phase structure of the coatings were tested by X-ray diffraction (XRD, DX-1000, Dandong Fangyuan Instrument CO., LTD.). Cu K_α incident radiation, a tube voltage of 35 kV and a current of 35 mA was used and the scanning angle is ranged from 20 to 60°, with a scan rate of (2θ) 0.06° s^{-1}. The functional groups present in the as-synthesized coatings were analyzed by Nicolet 670 FTIR Spectrometer (USA) over the range from 400 cm^{-1} to 4000 cm^{-1} with a number of scans 64 and resolution 4 cm^{-1}. The specimens were prepared by mixing 0.001 g of the deposit powder (scraped off from the Ti surface) together with 0.1 g of KBr to make a pellet.

To measure the quantity of copper/zinc precisely by inductively coupled plasma atomic emission spectrometer (ICP-AES; ICPS-100IV, SHIMADZU, Japan), the ZnCuHAP coatings were immersed in 200 g L^{-1} of chromium trioxide and 10 g L^{-1} of silver nitrate solution for 20 s. The samples was completely dissolved, the concentration of Ca^{2+}, Cu^{2+}, Zn^{2+} and PO_4^{3-}

dissolved from the coatings in the solution was detected with an ICP. An average of three measurements was taken for each sample.

The bond strength (BS) between the as-electrodeposited CuZnHAP coating and the Ti substrate was evaluated using an electronic universal testing machine, in accordance with the ASTM international standard F1044-05.[26,27] Three replicate tests were conducted. The counter Ti substrate was attached to the surface of the CuZnHAP coating using epoxy. After heating in an oven at 120 °C for 2 h, the samples were tested for tensile strength at a constant speed of 1 mm min^{-1} until fracture. Adhesive BS was calculated as failure load/sample area (0.785 cm^2).

2.3. Potentiodynamic polarisation assay

A simulated body fluid (SBF) solution was prepared according to ISO 23317:2007 using the procedure proposed by Kokubo *et al.*[31] The corrosion properties of the coatings in SBF were detected by potentiodynamic polarization tests at (37 ± 0.5) °C by employing an electrochemistry workstation controlled *via* a personal computer and software. The tests were conducted by adopting an initial delay time at the equilibrium state of 1 h to maintain the Ti-cp surface at open circuit potential. Electrochemical experiments were conducted for the Ti-cp, HAP-coated Ti-cp and ZnCuHAP-coated Ti-cp at a scan rate of 10 mV s^{-1}. All experimental potentials were associated with SCE, and all polarization parameters were normalised considering the working electrode area (100 mm^2). Each test was repeated for three times to evaluate reproducibility.

2.4. Antimicrobial activity test

E. coli was employed to analyse antimicrobial activity. Antimicrobial activity of the ZnCuHAP coating against *E. coli* was determined using plate-counting method. Before the test, all samples were sterilized at 121 °C for 20 min in an autoclave. The concentration of the bacterial solution was adjusted to 10^5 colony-forming unit (CFU) mL^{-1} with sterilized phosphate-buffered saline (PBS). Then, 30 μL of bacterial solutions were dripped separately on the surface of samples, and the samples were covered with an aseptic polyethylene film. After the samples were incubated with *E. coli* at 37 °C for 24 h, each sample was placed into a tube with 10 mL sterilized PBS (pH = 7.2), followed by shaking at 200 rpm for 5 min. A 100 μL portion of each shaken bacterial solution was respectively spread evenly on Luria–Bertani medium agar plates. The incubation period was conducted in a thermostat at 37 °C for 24 h, and then the visible cells of each plate were counted by quantifying the CFUs. Each test was performed in triplicate, and a witness test was also applied as a control group. Hence, the antimicrobial ratio (K) of the coatings was calculated using the formula:[32]

$$K = \frac{A - B}{A} \times 100$$

where A is the average number of colonies in the control and B is the average number of bacteria colonies in the ZnCuHAP or HAP coating.

2.5. Cytotoxicity test

MC3T3-E1 osteoblast-like cells from mouse skull (West China School of Medicine) were cultured at 37 °C in a humidified 5% CO_2 atmosphere in standard culture medium. The standard culture medium was Dulbecco's Modified Eagle Medium (DMEM, GIBCO), which consisted of α-minimal essential medium (Hyclone) supplemented with 10% foetal bovine serum (HyClone) and 1% penicillin/streptomycin (GIBCO). Upon reaching 85% to 90% confluence, the cells were separated by trypsin (Sigma-Aldrich), gathered and employed for cytotoxicity experiment. To evaluate the cytotoxicity of the ZnCuHAP coating, 2×10^4 cells per mL densities of MC3T3-E1 cells were seeded onto the samples. Cell adhesion test and MTT assay were performed according to previously described procedures,[25–30] which were based on previously established tests.[24,33]

2.6. Cu and Zn release rate tests

To examine Cu and Zn release, CuZnHAP coatings were statically incubated in a 24-well plate in 1 mL PBS at 37 °C and at varying time periods (1, 2, 4, and 7 days) in a humidified atmosphere. Three parallel samples were used for the ion release test. At each time interval, the solution was collected and replaced with 1 mL of fresh PBS. The Cu and Zn concentration of the collected solution was measured with an ICP.

2.7. Statistical analysis

Statistical analysis was performed using SPSS 19.0 software by one-way analysis ANOVA followed by Tukey–Kramer post hoc test. Statistical significance was considered at $p < 0.05$.

3. Results and discussion

3.1. Structural characterizations of the as-deposited coatings

XRD patterns of the as-deposited pure HAP and ZnCuHAP coatings are shown in Fig. 1A. XRD results confirmed the hexagonal HAP (space group $P6_3/m$; ICDD file: 00-009-0432) to be the main crystal phase in both coatings. The most intense diffraction peaks of the patterns were ascribed to the titanium peaks of the substrate (ICDD file: 00-044-1294). No other unwanted peaks were found in the as-synthesized specimens. In the case of as-deposited coatings, the broad and shallow ZnCuHAP peaks denote reduced crystallinity as well as particle size, owing to the incorporation of Cu/Zn in ZnCuHAP coating.[16,17] The diffraction peak at (0 0 2) plane was selected for local comparison because the plane was separated from other peaks.[25] Notably, for ZnCuHAP (Fig. 1B), the diffraction peak positions shifted towards higher angles from the standard XRD patterns for HAP. Both of the ionic radius (Cu^{2+}, 73 pm; Zn^{2+}, 74 pm) are smaller than that of Ca^{2+} ions, which is 100 pm. Therefore, co-substitution of Ca^{2+} by Cu/Zn ions leads to a contraction of the cell parameters of HAP.[34] The cell parameters have been calculated by XRD refinement method using Jade 5.0 software, as is shown in Table 1. So that both Zn and Cu ions will decrease the size of the unit cell of HA (528.80 $Å^3$ → 526.12 $Å^3$).

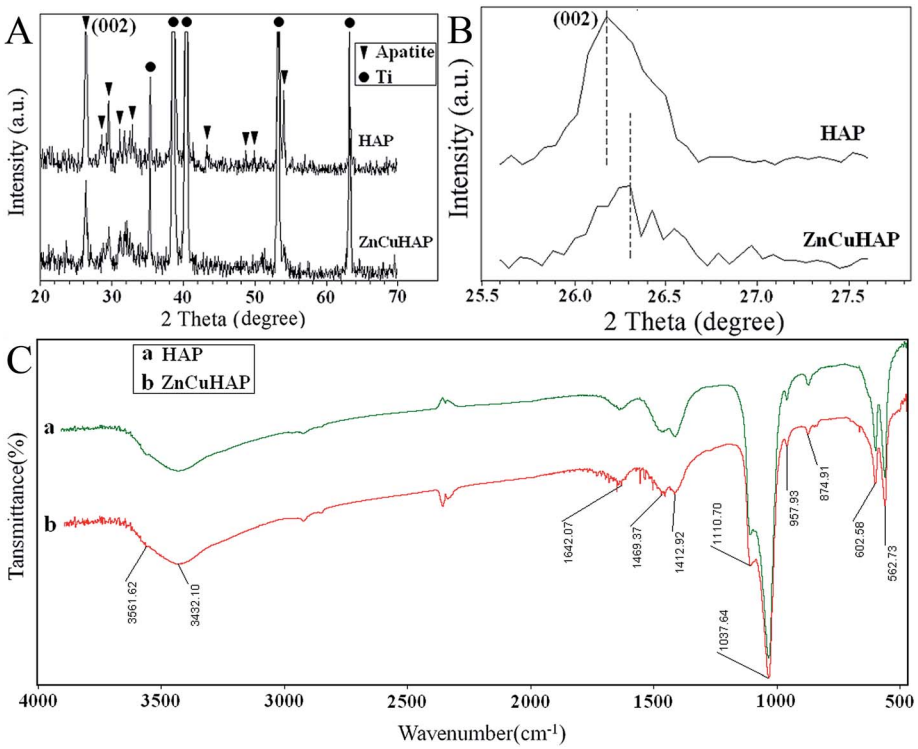

Fig. 1 (A) XRD patterns of HAP coating and ZnCuHAP coating on Ti-cp; (B) partial magnification of the XRD patterns; (C) FTIR spectra of the deposits scraped from the Ti-cp substrate.

The shift of XRD peaks with respect to Cu/Zn-free HAP served as evidence of Cu/Zn co-substitution in the obtained coatings.[35]

The unit cell of HAP contains 10 Ca^{2+} in two different locations: the Ca(I) site, in which 4 cations are connected with 9 oxygen atoms (Ca(I)–O distances: 0.241, 0.245 and 0.281 nm), and the Ca(II) site, in which 6 cations are connected with 7 oxygen atoms (Ca(II)–O distances: 0.236, 0.239 and 0.251 nm).[11] With a higher concentration of dopants, incorporation of Ca^{2+} in the Ca(II) site is mostly preferred, as represented by the substitution with Zn^{2+}, Sr^{2+}, Pb^{2+} and Cd^{2+}. However, with a lower concentration of dopants, incorporation of Ca^{2+} in the Ca(I) site is more favourable.[10] In the present study, the concentrations of the dopants Cu^{2+}/Zn^{2+} were low, and we supposed that substitution of Ca^{2+} in the Ca(I) site was favourable.

Fig. 1C shows the representative FTIR spectra of (a) HAP and (b) ZnCuHAP coatings deposited on Ti. Characteristic peaks [Fig. 1C(b)] appeared at 1110 and 1037 cm^{-1} (ν_3), 602 and 562 cm^{-1} (ν_4), as well as the band observed at 957 cm^{-1} (ν_1) assigned to the phosphate groups.[16,17] The ν_4 and ν_3 $(PO_4)^{3-}$ vibration bands are considered to be the IR fingerprint of a HAP structure.

Table 1 Lattice constant of HAP and ZnCuHAP

	$a = b$ (Å)	c (Å)	Vol (Å^3)
ZnCuHAP	9.391	6.879	526.12
HAP	9.418	6.884	528.80

The absorption peaks observed at 3561 cm^{-1} are assigned to the stretching vibration of OH– (hydroxyl) groups. Moreover, the broad stretching band at 3432 cm^{-1} and a bending peak at 1642 cm^{-1} are attributed to the H_2O molecule of ZnCuHAP coating, respectively. In particular, the peaks at 1459 (ν_2), 1412 (ν_2) and 874 (ν_3) cm^{-1} could be attributed to CO_3^{2-} replacing the PO_4^{3-} in HAP, thus forming the B-type carbonated HAP (CHAP).[25] The CO_3^{2-} originated from CO_2 in air, which dissolved in the electrolyte solution, and the B-type CHAP can normally be obtained from precipitation reaction.[36] Numerous studies have consistently revealed that CHAP typically shows superior bioactivity, cytocompatibility and, if porous, osteoconduction *in vivo*.[36] The FTIR spectrum of ZnCuHAP coating [Fig. 1C(b)] shows a similar structure as that of pure HAP [Fig. 1C(a)].[25,26,28] Slight changes in the shapes and intensities of the peaks were detected for ZnCuHAP coating, which suggest the lack of structural modification of HAP because the substitution of Cu/Zn was observed. This result is in accordance with the results reported by Shanmugam *et al.*[15] and Ding *et al.*[25] in 2014, in which FTIR examination of the CuHAP or ZnHAP did not provide confirmation of considerable change in the structure of pure HAP.

The typical surface morphologies of the HAP and ZnCuHAP coatings are investigated by FESEM, and the images are described in Fig. 2. FESEM images provide direct information on the size and shape of the deposited coatings. The HAP layer formed uniformly, with needle-like or flower cluster crystal morphology. These crystals fused together to form a microporous structure with pore diameter of approximately 2 μm to 4 μm. By contrast, the coatings obtained from Cu/Zn containing

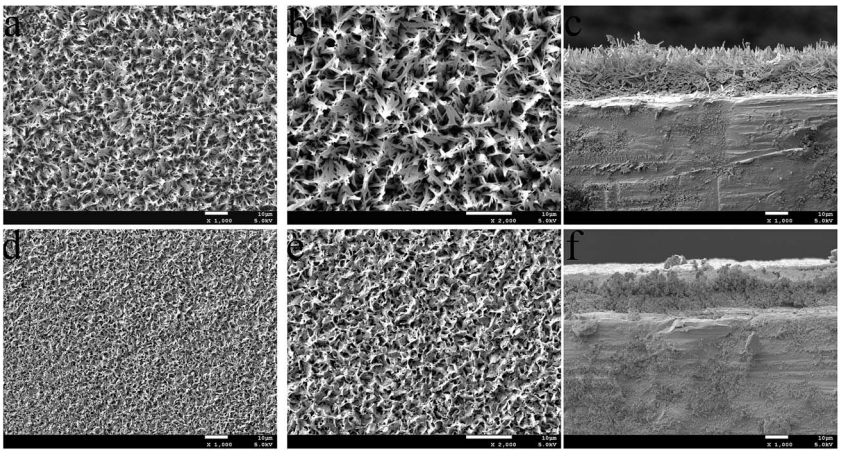

Fig. 2 SEM images of the (a and b) HAP coating and the (d and e) ZnCuHAP coating; Cross-section morphology of the (c) HAP coating and the (f) ZnCuHAP coating.

electrolytes showed a comparatively more compact appearance with smaller crystals (Fig. 2d), the dominant shape of which was flake-like (Fig. 2e). The co-substitution of (Cu/Zn) minerals in HAP increased the density, resulting in a relatively lower porosity (pore diameter, ≤1 μm) than the HAP coating. The decreased crystal size observed for depositions from Cu^{2+}/Zn^{2+} including electrolytes are possibly caused by a restricted growth of HAP crystals because of the positions of Cu and Zn species.[23,25] As shown in Fig. 2c and f, no apparent cracks or flaws that may induce fracture and shedding of the coating layer can be seen in the HAP and ZnCuHAP coatings, thus implying that both coatings were tightly bonded to the Ti-cp substrate. The thickness of the coatings was approximately 10 μm, which was suggested to be predominantly preferred for bone deposition.[26]

From a qualitative point of view, the EDS spectra of the HAP-based coatings (data not shown) revealed the existence of typical apatite elements only (Ca, P, O and C). As shown in Fig. 3 and in the case of ZnCuHAP coating, the presence of Cu and Zn was also emphasized, besides the characteristic HAP elements. The absence of other cations affirms the coating purity. EDS quantitative data were collected (inset in Fig. 3). A slight decrease of Ca/P atomic ratio in the HAP coatings (Ca/P = 1.41, data not shown) with respect to the theoretical HAP stoichiometry (Ca/P = 1.67), can be observed. Meanwhile, the Ca/P, Cu/P and Zn/P molar ratios of the ZnCuHAP coating were 1.30, 0.025 and 0.020, respectively. The decrease in Ca/P atomic ratio from 1.41 in HAP coating to 1.30 in ZnCuHAP coating confirms the replacement of a part of Ca ions by Cu/Zn ions.[25,30] These results suggest that the ZnCuHAP coating was Ca-deficient with a few Cu (~1.22 wt%) and Zn (~1.02 wt%) co-substitution (Fig. 4). Thus, 3.49 at.% of Ca ions have been substituted.

The determination of Cu/Zn quantity by EDS is insufficient, considering that EDS is only a semi-quantitative method. Precise measurement of Cu/Zn quantity is necessary because of their crucial antibacterial/cytotoxicity properties. Methods such as ICP would be useful for the precise measurement of Cu/Zn quantity. The results of ICP showed that the Ca/P, Cu/P and Zn/P atomic ratios of ZnCuHAP coating were 1.35, 0.019 and 0.018, respectively. These results suggest that ZnCuHAP coating

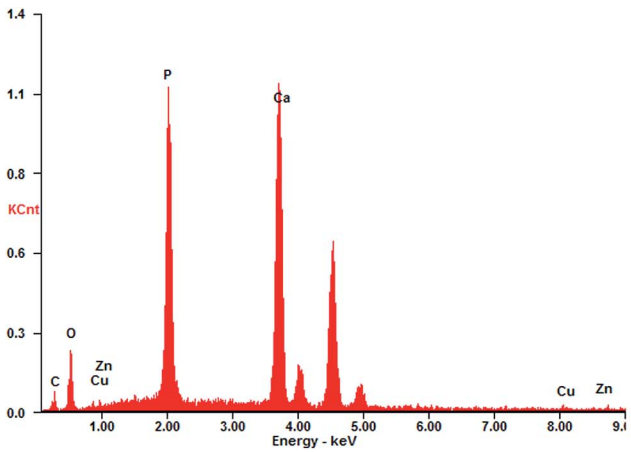

Element	Wt %	At %
CK	10.83	21.63
OK	23.65	35.48
PK	23.63	18.31
CaK	39.66	23.75
CuK	01.22	00.46
ZnK	01.02	00.37
Matrix	Correction	ZAF

Fig. 3 EDS elemental spectrum of the ZnCuHAP coating.

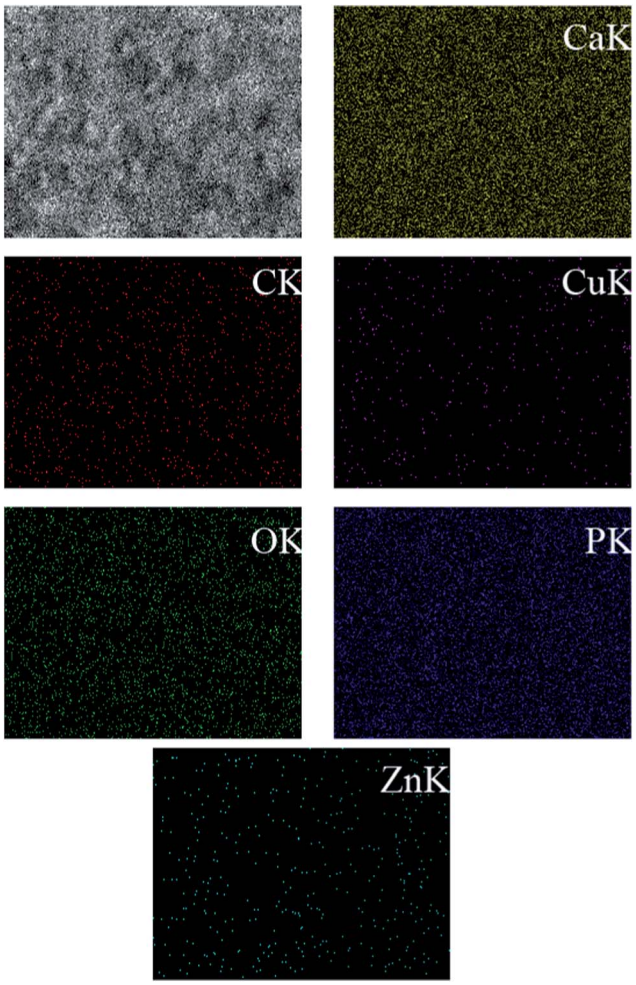

Fig. 4 EDS mapping of the lateral distribution of Zn, Cu, Ca, P, and O compared to the SEM image of the same area for ZnCuHAP coating.

was Ca-deficient with a low degree of Cu (~1.01 wt%) and Zn (~0.92 wt%) co-substitution. The Cu/Zn quantities are nearly consistent with the EDS results.

Fig. 4 demonstrates the lateral distribution of the elements Zn, Cu, Ca, P and O in comparison with the surface topography that exemplifies ZnCuHAP coating. The distribution patterns of all elements extremely correlates with the surface morphology, as the X-ray quanta originating from exposed surface sites are detected to a higher percentage than those from deeper structures, which are scattered to a larger degree. Given that the electrodeposited layer was quite uniform (Fig. 2d and e), a homogenous deposition of Cu and Zn species within the coating can be deduced. However, locating the precise position of Cu and Zn species in relation to the HAP flakes *via* EDS is impossible, as the lateral resolution ranges between 1 and 2 μm.[23]

The adhesion of the CuZnHAP coating to the Ti substrate is significant for the implant to function suitably in physiological conditions. In this study, the adhesion strength of the HAP and CuZnHAP coatings on Ti substrate was evaluated. The BS measured for the CuZnHAP film was 9.4 ± 2.7 MPa, with is slightly higher than 8.1 ± 2.1 MPa for pure HAP film. This BS value of the composite coating was consistent with previous

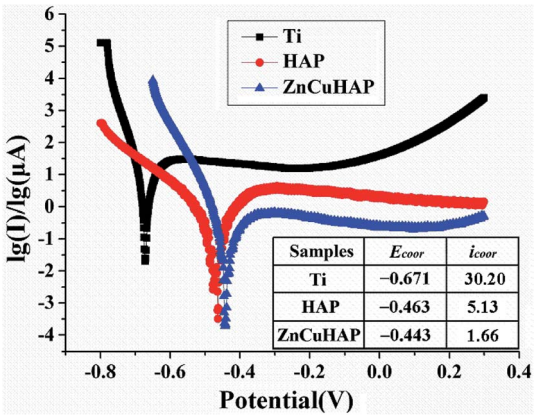

Fig. 5 The polarisation curves of the bare Ti and the Ti coated with coatings in SBF.

reports regarding SrHAP coating prepared by a traditional electrolytic deposition process (9.3 ± 0.7 MPa).[7] Evidently, the adhesive BS was not affected by the co-substitution of Zn^{2+} and Cu^{2+} ions. This adhesion strength of the as-formed composite coating will make the material suitable for orthopaedic applications.

3.2. Corrosion behaviour

Fig. 5 shows the potentiodynamic scan of the uncoated, HAP-coated and ZnCuHAP-coated Ti-cp in SBF. For comparison, corrosion current density (i_{corr}) and corrosion potential (E_{corr}) calculated from potentiodynamic curves using Tafel extrapolation method[8] are listed as an inset in Fig. 5. The curves of the specimens shifted to a nobler E_{corr} and a lower i_{corr}. The corrosion rate of a material proportional to the i_{corr} at a given potential, and materials with higher value of i_{corr} material is more prone to corrosion.[6,7]

Compared with the uncoated specimen, the HAP coating enhanced the corrosion potential by 208 mV, and the i_{corr} was decreased by one order of magnitude. For the ZnCuHAP-coated specimen, the polarization curve moved to the right (lower i_{corr}, 1.66 μA cm^{-2}) and downward (higher E_{corr}, −0.443 V), revealing that the corrosion resistance of Ti-cp substrate was further enhanced by ZnCuHAP coating. The films restricted penetration of the solution into the bulk substrate, thereby blocking the infiltration of chloride ions to the Ti-cp substrate. Earlier corrosion studies on ionic-doped HAP coatings show the same results.[6,7] In the present study, the ZnCuHAP coating was prepared on Ti-cp substrate, consequently decreasing the specific surface because of the formation of a denser coating, as proven by the FESEM micrograph in Fig. 2. The reduced grain size has a distinguishing feature in elevating electron activity at the grain boundaries,[26] thus decreasing i_{corr}, which translates to improved corrosion protection.

3.3. Antimicrobial assessment

The results of the quantitative antibacterial tests are presented in Fig. 6. Antimicrobial ratio (K) was calculated from the number of colonies after 24 h incubation periods and listed as an inset in Fig. 6. The ZnCuHAP coating showed the highest

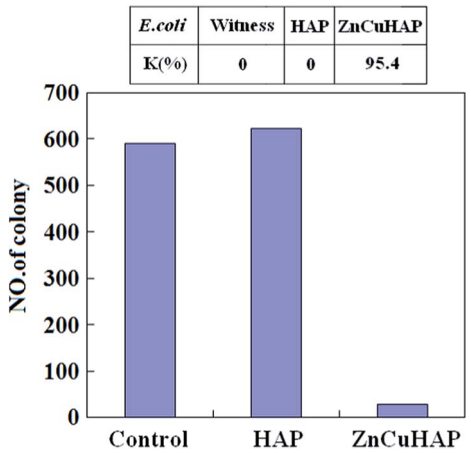

Fig. 6 Antimicrobial activity of the HAP and ZnCuHAP coating.

activity against *E. coli* in comparison with the HAP coating and the control. Antimicrobial results revealed that Cu ions released from ZnCuHAP present a strong bactericidal effect against these organisms (antimicrobial ratio > 95%). This enhancement may be due to the high release of copper in ZnCuHAP in the PBS medium after 24 h incubation (based on the ICP-AES analysis).

The antibacterial tests results revealed that pure HAP coating has no antibacterial property. The pure HAP plate showed more colonies than the control sample (Fig. 6). This finding showed that proteins, amino acids, and other organic matter are readily adsorbed on the HAP surface, which could favour adsorption and replication of bacteria on the coating, usually causing implant-related infections.[37] Therefore, endowing antimicrobial properties to HAP is necessary. Several recent studies have introduced antimicrobial activity of materials that involve Cu(II) ions. Du *et al.*[38] have suggested that chitosan nanoparticles loaded with Cu(II) ions interact with bacterial cell membranes of *E. coli*, causing structural changes and, eventually, cell death. Nan *et al.*[39] also suggested that structure of the outer cell membrane responsible for cell permeability is significantly altered for *E. coli* after contact with antimicrobial stainless steel with Cu(II) ions. This finding indicates that cell walls were badly undermined, and numerous cellular contents are released. Notably, Zn ions released from ZnCuHAP may also exhibit antimicrobial activity, thus preventing and minimizing initial bacterial adhesion.[16,17] Kai Li *et al.*[40] showed that Zn-doped HAP could inhibit surface growth of bacteria, such as *Staphylococcus aureus* and *E. coli*, and discussed the antibacterial mechanism. It has been reported that Zn released within 0.26 μg mL^{-1} (0.26 ppm) in the culture medium is antimicrobic.[1] In this work, the released Zn ions were measured by ICP-AES, and the highest accumulated Zn ion concentration within 7 days immersion is 0.77 μg cm^{-2} (Fig. 9), which is a little more than 0.26 μg mL^{-1}. Apparently, the concentration of Zn ions can reach to the antimicrobial level.

3.4. *In vitro* cytotoxicity studies with MC3T3-E1 cells

The SEM images (Fig. 7) indicated differences in cell density and spreading patterns among the MC3T3-E1 cells grown on the apatite-coated and non-coated Ti-cp substrates after 24 h. The results demonstrated that cells spread well onto all surfaces and exhibited active cytoskeletal extension. In Fig. 7c–f, the osteoblasts on ZnCuHAP notably appeared even more flattened and evenly spread across the coating surface than on HAP, which reveals the absence of a toxic nature. Interestingly, on the Ti-cp surface (Fig. 7a and b), cell density was similar to that on the apatite-coated specimens, indicating that all three specimens demonstrated sufficiently high cell viability after 24 h of incubation.

The cytotoxicity of ZnCuHAP coating was evaluated by MTT test (Fig. 8). After one day culture, the cell number did not significantly differ between the Ti-cp and the coated specimens (ZnCuHAP and HAP coatings), which was in agreement with cell adhesion results (Fig. 7). During the next two periods (4 and 7 days), the cell numbers on Ti-cp were significantly lower ($p < 0.05$) than those on the coated specimens, revealing that the ZnCuHAP and HAP coatings had higher cytocompatibility than the Ti-cp. No remarkable difference ($p > 0.05$) was found between ZnCuHAP and HAP coatings after 4 days of culture. In addition, after 7 days, the cell numbers on the ZnCuHAP coating were significantly higher ($p < 0.05$) than those on the HAP coating. These results showed that the obtained HAP coating doped with lower Cu^{2+} (1.22 wt%) and Zn^{2+} (1.02 wt%) contents showed good cytocompatibility, presented no cytotoxicity towards osteoblast cells, and was favourable for implant

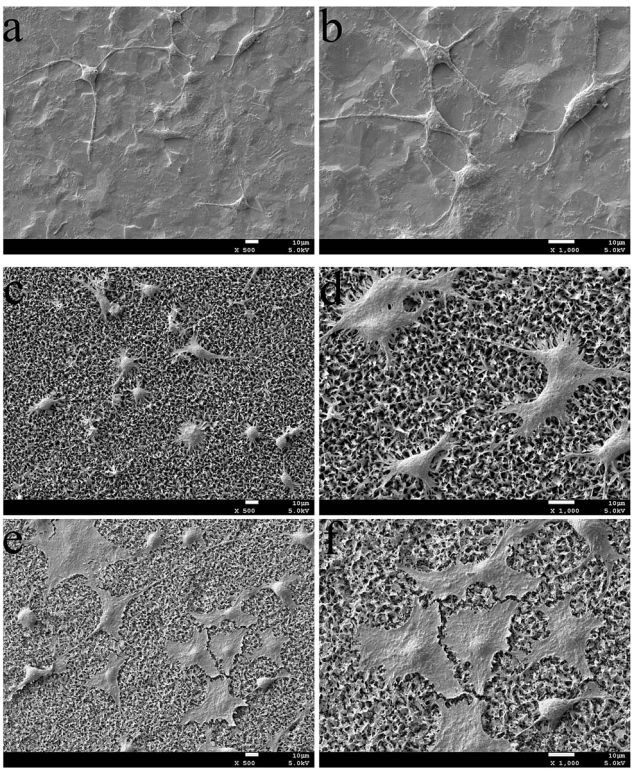

Fig. 7 SEM morphologies of the MC3T3-E1 cells grown on bare Ti substrate (a), HAP coating (c) and ZnCuHAP coating (e); The higher magnification images of the surface of the MC3T3-E1 cells grown on bare Ti substrate (b), HAP coating (d) and ZnCuHAP coating (f).

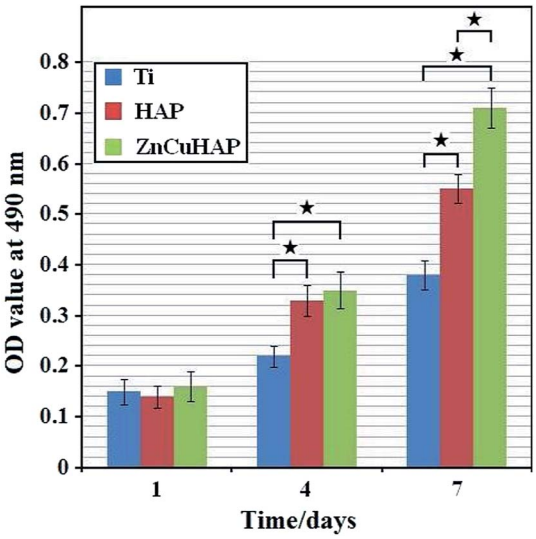

Fig. 8 OD measurements illustrating MC3T3-E1 cell proliferation on the ceramic coatings and bare Ti substrate after culturing for 1, 4 and 7 days (one-way ANOVA, ★, $p < 0.05$).

applications. However, such concentration of Cu must also exert an antibacterial effect by restraining bacterial growth to prevent microbial infections when used as *in vivo* implants.

The target coating surface does not release any toxic ions that could injure the cells involved in osteogenesis. Gbureck *et al.*[41] revealed that Cu(II) improves cell activity and proliferation of osteoblasts on calcium phosphate cements and affects the expression of several special osteogenic proteins, such as bone sialo protein or osteocalcin. Therefore, the modification of calcium phosphate cements with Cu may provide a likely alternative to protein-based modification to promote cell viability for superior bone healing. Although Cu is known to be a preferred antibacterial agent, high concentrations of copper ions cause cytotoxicity.[20] Li *et al.*[42] fabricated CuHAP using ionic exchange process; this material exhibited high antibacterial potency against *E. coli* but was proved to be cytotoxic to human fetus osteoblasts. Thus, to achieve a good balance between cell biomaterial interaction and antimicrobial properties, a biomaterial with better bone bonding capacity (*i.e.*, Zn) is co-substituted in CuHAP to offset the cytotoxicity of higher Cu concentration and stimulate osteogenic growth.[17]

Furthermore, numerous studies have shown that Zn-substituted HAP coating could release trace Zn^{2+} in the degradation process, which was advantageous in stimulating cell proliferation.[21,25,43–45] Ito *et al.*[46] showed that doping with Zn in certain amounts (between 0.6 and 1.2 wt%) in a tricalcium phosphate/HAP composite ceramic improved the proliferation of murine osteoblasts; even extremely low amounts of Zn (0.012 wt% to 0.025 wt% in human bone) present a stimulating effect in the formation of bone *in vitro* and *in vivo*.[47–49] Wang *et al.*[50] fabricated ZnHAP coating on Ti-cp rods, which remarkably increased fibroblast proliferation.

Zinc is important for cell proliferation, and can stimulate osteogenesis, inhibit osteoclastogenesis and induce bone formation. The ICP-AES results indicate that the released Zn concentration increases with implantation time (Fig. 9), and the highest accumulated Zn ion concentration within 7 days immersion is 0.77 μg cm^{-2}. Previous studies have shown that osteoblasts are the major organization forming cells in the process of osseointegration, and osteoblasts are widely used in tissue engineering bone. In this work, the ZnCuHAP surfaces are favorable for the proliferation of MC3T3-E1 cells, the numbers of cells on the ZnCuHAP surfaces are obviously higher than HAP, while the cell morphologies show that cells grow well on the ZnCuHAP surfaces. As stated above, Zn is beneficial to biological performance. Considering the similar microstructure, surface roughness and wettability of CuHAP and ZnCuHAP,[51] the implantation of Zn is considered to be the main reason for the increased proliferation of MC3T3-E1 cells. Moreover, the released Zn ions within 7 days' immersion shows that Zn concentration increases with implantation time, which is consistent with the proliferation of MC3T3-E1 cells, suggesting that the released Zn ions is the main factor that influence the proliferation of MC3T3-E1 cells.

It is believed that Zn ions at an appropriate concentration is a factor to promote osteoblast functions, bone formation, and has partly antibacterial effect on bacteria without introducing undesired side effect. Form an overall perspective, it can be concluded that the enhanced proliferation of MC3T3-E1, initial adhesion and spreading activity, and partly antibacterial effect of the ZnCuHAP coating are due to the released Zn ions. All of the above results suggested that the as-deposited ZnCuHAP coating has the potential to decrease bacterial adhesion to the surface of Ti implants while maintaining healthy osteoblast cellular activity.

3.5. Investigation on the release behaviour of Cu/Zn

After confirming the formation of Cu/Zn ions co-substituted HAP coating, we measured the time course release of Cu/Zn ions (Fig. 9). The release of Cu and Zn ions from CuZnHAP coatings exhibits sustained release kinetics without burst release. The total quantity of released Cu species ranged from 0.12 μg to 0.61 μg per cm^2 of sample surface, and the total

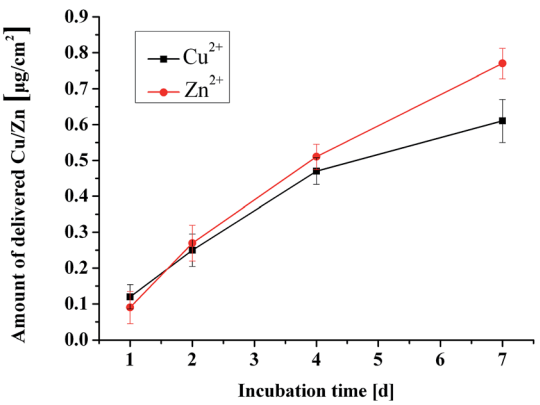

Fig. 9 Amount of delivered copper/zinc species per surface area, static incubation, 37 °C in PBS.

quantity of released Zn species ranged from 0.09 μg to 0.77 μg per cm^2 (Fig. 9). Notably, the release kinetics of Cu/Zn was nearly linear. The coatings showed a high release rate within the first week, suggesting that Cu/Zn-containing coatings can provide a continuous Cu and Zn ion release platform. The subsequent release of Cu ions improves the antibacterial ability of the HAP coating, and this concentration of Cu ions that were released from the coatings exhibits no toxicity towards osteoblasts. Meanwhile, this sustained high Zn ion release into the microenvironment around the implant/tissue interface generally regulates the cell behaviour in a positive manner. Results from MTT assay show that CuZnHAP coatings are more favourable for osteoblast proliferation compared with pure HAP coatings.

4. Conclusions

In summary, novel antibacterial and biocompatible ZnCuHAP coatings were synthesized by electrodeposition method. The non-cytotoxic coatings showed good antibacterial efficacy and corrosion resistance. The co-doping of Cu^{2+} and Zn^{2+} into HAP slightly reduced the porosity, and the coating became denser. Potentiodynamic polarisation studies showed that the ZnCuHAP coating on Ti-cp possesses superior corrosion resistance in SBF. The substitution of Cu in HAP significantly enhanced the antibacterial activity of HAP. Simultaneously, co-substitution of Zn in CuHAP coating offsets the possible toxic nature of Cu, thereby promoting the cell viability. Thus, a good balance between MC3T3-E1 cell material interaction and antibacterial property was achieved in ZnCuHAP. Given the antibacterial property and biocompatibility of the as-prepared ZnCuHAP coating, it is a potential candidate for biomedical applications.

Acknowledgements

This work was supported by the National Basic Research Program of China ("973" Program, no. 2011CB503700).

References

1 G. D. Jin, H. L. Cao, Y. Q. Qiao, F. H. Meng, H. Q. Zhu and X. Y. Liu, Osteogenic activity and antibacterial effect of zinc ion implanted titanium, *Colloids Surf., B*, 2014, **117**, 158–165.

2 S. Kalaivani, R. K. Singh, V. Ganesan and S. Kannan, Effect of copper (Cu^{2+}) inclusion on the bioactivity and antibacterial behavior of calcium silicate coatings on titanium metal, *J. Mater. Chem. B*, 2014, **2**, 846–858.

3 L. Yu, S. Qian, Y. Q. Qiao and X. Y. Liu, Multifunctional Mn-containing titania coatings with enhanced corrosion resistance, osteogenesis and antibacterial activity, *J. Mater. Chem. B*, 2014, **2**, 5397–5408.

4 S. Facca, D. Lahiri, F. Fioretti, N. Messadeq, D. Mainard, N. Benkirane-Jessel and A. Agarwal, In Vivo Osseointegration of Nano-Designed Composite Coatings on Titanium Implants, *ACS Nano*, 2011, **5**, 4790–4799.

5 Y. C. Xin, J. Jiang, K. F. Huo, T. Hu and P. K. Chu, Bioactive $SrTiO_3$ Nanotube Arrays: Strontium Delivery Platform on Ti-Based Osteoporotic Bone Implants, *ACS Nano*, 2009, **3**, 3228–3234.

6 D. Gopi, A. Karthika, D. Rajeswari, L. Kavitha, R. Pramodd and J. Dwivedi, Investigation on corrosion protection and mechanical performance of minerals substituted hydroxyapatite coating on HELCDEB-treated titanium using pulsed electrodeposition method, *RSC Adv.*, 2014, **4**, 34751–34759.

7 D. Gopi, N. Murugan, S. Ramya and L. Kavitha, Electrodeposition of a porous strontium substituted hydroxyapatite/zinc oxide duplex layer on AZ91 magnesium alloy for orthopedic applications, *J. Mater. Chem. B*, 2014, **2**, 5531–5540.

8 M. M. Ren, S. Cai, T. L. Liu, K. Huang, X. X. Wang, H. Zhao, S. X. Niu, R. Y. Zhang and X. D. Wu, Calcium phosphate glass/MgF_2 double layered composite coating for improving the corrosion resistance of magnesium alloy, *J. Alloys Compd.*, 2014, **591**, 34–40.

9 N. J. Shah, J. Hong, M. N. Hyder and P. T. Hammond, Osteophilic Multilayer Coatings for Accelerated Bone Tissue Growth, *Adv. Mater.*, 2012, **24**, 1445–1450.

10 W. Chen, T. Long, Y. J. Guo, Z. A. Zhu and Y. P. Guo, Magnetic hydroxyapatite coatings with oriented nanorod arrays: hydrothermal synthesis, structure and biocompatibility, *J. Mater. Chem. B*, 2014, **2**, 1653–1660.

11 D. E. Ellis, J. Terra, O. Warschkow, M. Jiang, G. B. González and J. S. Okasinski, *et al.*, A theoretical and experimental study of lead substitution in calcium hydroxyapatite, *Phys. Chem. Chem. Phys.*, 2006, **28**, 967–976.

12 A. A. El hadad, V. Barranco, A. Jimenez-Morales, E. Peon, G. J. Hickman, C. C. Perry and J. C. Galvan, Enhancing in vitro biocompatibility and corrosion protection of organic–inorganic hybrid sol–gel films with nanocrystalline hydroxyapatite, *J. Mater. Chem. B*, 2014, **2**, 3886–3896.

13 R. Kargupta, S. Bok, C. M. Darr, B. D. Crist, K. Gangopadhyay, S. Gangopadhyay and S. Sengupta, Coatings and surface modifications imparting antimicrobial activity to orthopedic implants, *WIREs Nanomedicine and Nanobiotechnology*, 2014, **6**, 475–495.

14 A. Mocanu, G. Furtos, S. Rapuntean, O. Horovitz, C. Flore and C. Garbo, *et al.*, Synthesis; characterization and antimicrobial effects of composites based on multi-substituted hydroxyapatite and silver nanoparticles, *Appl. Surf. Sci.*, 2014, **298**, 225–235.

15 S. Shanmugam and B. gopal, Copper substituted hydroxyapatite and fluorapatite: synthesis, characterization and antimicrobial properties, *Ceram. Int.*, 2014, **40**, 15655–15662.

16 D. Gopi, S. Ramya, D. Rajeswari, P. Karthikeyan and L. Kavitha, Strontium, cerium co-substituted hydroxyapatite nanoparticles: Synthesis, characterization, antibacterial activity towards prokaryotic strains and *in vitro* studies, *Colloids Surf., A*, 2014, **451**, 172–180.

17 D. Gopi, E. Shinyjoy and L. Kavitha, Synthesis and spectral characterization of silver/magnesium co-substituted hydroxyapatite for biomedical applications, *Spectrochim. Acta, Part A*, 2014, **127**, 286–291.

18 Z. Radovanovic, B. Jokic, D. Veljovic, S. Dimitrijevic, V. Kojic and R. Petrovic, *et al.*, Antimicrobial activity and biocompatibility of Ag^{+}- and Cu^{2+}-doped biphasic hydroxyapatite/α-tricalcium phosphate obtained from hydrothermally synthesized Ag^{+}- and Cu^{2+}-doped hydroxyapatite, *Appl. Surf. Sci.*, 2014, **307**, 513–519.

19 P. Habibovic and J. E. Barralet, Bioinorganics and biomaterials: Bone repair, *Acta Biomater.*, 2011, **7**, 3013–3026.

20 L. Yang, S. Perez-Amodio, F. Y. F. Barrere-de Groot, V. Everts, C. A. van Blitterswijk and P. Habibovic, The effects of inorganic additives to calcium phosphate on in vitro behavior of osteoblasts and osteoclasts, *Biomaterials*, 2006, **31**, 2976–2989.

21 Z. T. Chen, D. L. Yi, X. B. Zheng, J. Chang, C. T. Wu and Y. Xiao, Nutrient element-based bioceramic coatings on titanium alloy stimulating osteogenesis by inducing beneficial osteoimmmunomodulation, *J. Mater. Chem. B*, 2014, **2**, 6030–6043.

22 E. Mohseni, E. Zalnezhad and A. R. Bushroa, Comparative investigation on the adhesion of hydroxyapatite coating on Ti–6Al–4V implant: A review paper, *Int. J. Adhes. Adhes.*, 2014, **48**, 238–257.

23 C. Wolf-Brandstetter, S. Oswald, S. Bierbaum, H. P. Wiesmann and D. Scharnweber, Influence of pulse ratio on codeposition of copper species with calcium phosphate coatings on titanium by means of electrochemically assisted deposition, *J. Biomed. Mater. Res., Part B*, 2014, **102**, 160–172.

24 L. L. Zhang, H. J. Li, K. Z. Li, S. Y. Zhang, Q. G. Fu and Y. L. Zhang, *et al.*, Preparation and characterization of carbon/SiC nanowire/Na-dopedcarbonated hydroxyapatite multilayer coating for carbon/carboncomposites, *Appl. Surf. Sci.*, 2014, **313**, 85–92.

25 Q. Q. Ding, X. J. Zhang, Y. Huang, Y. J. Yan and X. F. Pang, *In vitro* cytocompatibility and corrosion resistance of zinc-doped hydroxyapatite coatings on a titanium substrate, *J. Mater. Sci.*, 2015, **50**, 189–202.

26 Y. Huang, Q. Q. Ding, S. G. Han, Y. J. Yan and X. F. Pang, Characterisation, corrosion resistance and *in vitro* bioactivity of manganese-doped hydroxyapatite films electrodeposited on titanium, *J. Mater. Sci.: Mater. Med.*, 2014, **24**, 1853–1864.

27 Y. Huang, Y. J. Yan and X. F. Pang, Electrolytic deposition of fluorine-doped hydroxyapatite/ZrO_2 films on titanium for biomedical applications, *Ceram. Int.*, 2013, **39**, 245–253.

28 Y. Huang, Y. J. Yan, X. F. Pang, Q. Q. Ding and S. G. Han, Bioactivity and corrosion properties of gelatin-containing and strontium-doped calcium phosphate composite coating, *Appl. Surf. Sci.*, 2013, **282**, 583–589.

29 Y. J. Yan, Q. Q. Ding, Y. Huang, S. G. Han and X. F. Pang, Magnesium substituted hydroxyapatite coating on titanium with nanotublar TiO_2 intermediate layer via electrochemical deposition, *Appl. Surf. Sci.*, 2014, **305**, 77–85.

30 Y. J. Yan, X. J. Zhang, Y. Huang, Q. Q. Ding and X. F. Pang, Antibacterial and bioactivity of silver substituted hydroxyapatite/TiO_2 nanotube composite coatings on titanium, *Appl. Surf. Sci.*, 2014, **314**, 348–357.

31 T. Kokubo and H. Takadama, How useful is SBF in predicting in vivo bone bioactivity?, *Biomaterials*, 2006, **27**, 2907–2915.

32 S. Shanmugam and B. Gopal, Synthesis; Antimicrobial and cytotoxicity evaluation of aliovalent substituted hydroxyapatite, *Appl. Surf. Sci.*, 2014, **303**, 277–281.

33 X. B. Pei, Y. X. Zeng, R. He, Z. J. Li, L. Y. Tian and J. Wang, *et al.*, Single-walled carbon nanotubes/hydroxyapatite coatings on titanium obtained by electrochemical deposition, *Appl. Surf. Sci.*, 2014, **295**, 71–80.

34 U. Batra, S. Kapoor and S. Sharma, Influence of magnesium ion substitution on structural and thermal behavior of nanodimensional hydroxyapatite, *J. Mater. Eng. Perform.*, 2012, **22**, 1798–1806.

35 W. Hu, J. Ma, J. G. Wang and S. M. Zhang, Fine structure study on low concentration zinc substituted hydroxyapatite nanoparticles, *Mater. Sci. Eng., C*, 2012, **32**, 2404–2410.

36 L. L. Zhang, H. J. Li, K. Z. Li, Q. G. Fu, Y. L. Zhang and S. J. Liu, A Na and Si co-substituted carbonated hydroxyapatite coating for carbon nanotubes coated carbon/carbon composites, *Ceram. Int.*, 2014, **40**, 13123–13130.

37 X. M. Liu, Y. N. Mou, S. L. Wu and H. C. Man, Synthesis of silver-incorporated hydroxyapatite nanocomposites for antimicrobial implant coatings, *Appl. Surf. Sci.*, 2013, **273**, 748–757.

38 W. L. Du, Y. L. Xu, Z. R. Xu and C. L. Fan, Preparation, characterization and antibacterial properties against *E. coli* K_{88} of chitosan nanoparticle loaded copper ions, *Nanotechnology*, 2008, **19**, 085707.

39 L. Nan, Y. Liu, M. Lü and K. Yang, Study on antibacterial mechanism of copper bearing austenitic antibacterial stainless steel by atomic force microscopy, *J. Mater. Sci.: Mater. Med.*, 2008, **19**, 3057–3062.

40 K. Li, Y. T. Xie, H. Y. Ao, L. P. Huang, H. Ji and X. B. Zheng, The enhanced bactericidal effect of plasma sprayed zinc-modified calcium silicate coating by the addition of silver, *Ceram. Int.*, 2013, **39**, 7895–7902.

41 A. Ewald, C. Kappel, E. Vorndran, C. Moseke, M. Gelinsky and U. Gbureck, The effect of Cu(II)-loaded brushite scaffolds on growth and activity of osteoblastic cells, *J. Biomed. Mater. Res., Part A*, 2012, **100**, 2392–2400.

42 Y. Li, J. Ho and C. P. Ooi, Antibacterial efficacy and cytotoxicity studies of copper(II) and titanium(IV) substituted hydroxyapatite nanoparticles, *Mater. Sci. Eng., C*, 2010, **30**, 1137–1144.

43 E. H. Alcantara, M. Y. Shin, J. Feldmann, G. F. Nixon, J. H. Beattie and I. S. Kwun, Long-term zinc deprivation accelerates rat vascular smooth muscle cell proliferation involving the down-regulation of JNK1/2 expression in MAPK signaling, *Atherosclerosis*, 2013, **228**, 46–52.

44 S. Horiuchi, M. Hiasa, A. Yasue, K. Sekine, K. Hamada and K. Asaoka, *et al.* Fabrications of zinc-releasing biocement combining zinc calcium phosphate to calcium phosphate cement, *J. Mech. Behav. Biomed. Mater.*, 2014, **29**, 151–160.

45 Y. Hondal, T. Anada, S. Morimoto and O. Suzuki, Labile Zn ions on octacalcium phosphate-derived Zn-containing hydroxyapatite surfaces, *Appl. Surf. Sci.*, 2013, **273**, 343–348.
46 A. Ito, K. Ojima, H. Naito, N. Ichinose and T. Tateishi, Preparation, solubility, and cytocompatibility of zinc-releasing calcium phosphate ceramics, *J. Biomed. Mater. Res.*, 2000, **50**, 178–183.
47 F. Ren, R. Xin, X. Ge and Y. Leng, Characterization and structural analysis of zinc-substituted hydroxyapatites, *Acta Biomater.*, 2009, **5**, 3141–3149.
48 Y. Tang, H. F. Chappell, M. T. Dove, R. J. Reeder and Y. J. Lee, Zinc incorporation into hydroxylapatite, *Biomaterials*, 2009, **30**, 2864–2872.
49 D. Gopi, A. Karthika, S. Nithiya and L. Kavitha, In vitro biological performance of minerals substituted hydroxyapatite coating by pulsed electrodeposition method, *Mater. Chem. Phys.*, 2014, **144**, 75–85.
50 X. Wang, A. Ito, Y. Sogo, X. Li and A. Oyane, zinc-containing apatite layers on external fixation rods promoting cell activity, *Acta Biomater.*, 2010, **6**, 962–968.
51 Y. Huang, X. J. Zhang, R. L. Zhao, H. H. Mao, Y. J. Yan and X. F. Pang, Antibacterial efficacy, corrosion resistance, and cytotoxicity studies of copper-substituted carbonated hydroxyapatite coating on titanium substrate, *J. Mater. Sci.*, 2015, **50**, 1688–1700.